Author Manuscript

Author Manuscript

Author Manuscript

Author Manuscript

HHS Public Access

Author manuscript

Matrix Biol. Author manuscript; available in PMC 2020 October 11.

Engineering microenvironment for human cardiac tissue assembly in heart-on-a-chip platform

Yimu Zhao[1], **Naimeh Rafatian**[2], **ErikaY. Wang**[3], **Nicole T. Feric**[4], **Benjamin F. L. Lai**[3], **Ericka J. Knee-Walden**[3], **Peter H. Backx**[5], **Milica Radisic**[6,*]

[1]Department of Chemical Engineering and Applied Chemistry; University of Toronto; Toronto; Ontario, M5S 3E5; Canada.

[2]Division of Cardiology and Peter Munk Cardiac Center; University of Health Network; Toronto; Ontario, M5G 2N2; Canada.

[3]Institute of Biomaterials and Biomedical Engineering; University of Toronto; Toronto; Ontario, M5S 3G9; Canada.

[4]Institute of Biomaterials and Biomedical Engineering, University of Toronto, Toronto, Ontario M5S 3G9, Canada; TARA Biosystems, Inc., New York, NY 10016, USA.

[5]Division of Cardiology and Peter Munk Cardiac Center, University of Health Network, Toronto, Ontario M5G 2N2, Canada; Department of Physiology, Faculty of Medicine, University of Toronto, Toronto, Ontario M5S 1A8, Canada; Department of Biology, York University, Toronto, Ontario M3J 1P3, Canada; Toronto General Research Institute, Toronto, Ontario M5G 2C4; Canada.

[6]Department of Chemical Engineering and Applied Chemistry, University of Toronto, Toronto, Ontario M5S 3E5; Canada; Institute of Biomaterials and Biomedical Engineering, University of Toronto, Toronto, Ontario M5S 3G9, Canada; Toronto General Research Institute, Toronto, Ontario M5G 2C4; Canada.

[*]Correspondence: Milica Radisic m.radisic@utoronto.ca, Rm407, Rosebrugh Building, Institute of Biomaterials and Biomedical Engineering;, University of Toronto; Toronto; Ontario, M5S 3G9; Canada.

Author Contribution:
Conceptualization, Y.Z and M.R.;
Methodology, Y.Z, N.R., P.H.B. and M.R.;
Validation, Y.Z, N.R., N.F., E.Y.W., B.F.L.L., E.J.K., P.H.B. and M.R.;
Formal Analysis, Y.Z, N.R.
Investigation, Y.Z,
Resources, P.H.B., M.R.
Data Curation, Y.Z., N.R., P.H.B. and M.R.,
Writing – Original Draft, Y.Z., M.R.;
Writing – Review & Editing, N.F., B.F.L.L., M.R., P.H.B.,
Visualization, Y.Z., E.Y.W. and M.R.;
Supervision, M.R.;
Project Administration, Y.Z and M.R.;
Funding Acquisition, M.R.

Publisher's Disclaimer: This is a PDF file of an unedited manuscript that has been accepted for publication. As a service to our customers we are providing this early version of the manuscript. The manuscript will undergo copyediting, typesetting, and review of the resulting proof before it is published in its final citable form. Please note that during the production process errors may be discovered which could affect the content, and all legal disclaimers that apply to the journal pertain.

Conflict of interest disclosure: Y.Z. and M.R. are co-founders of TARA Biosystems Inc, and hold equity in this company. NF is an employee and a shareholder of the company. TARA Biosystems Inc, uses the Biowire II technology described in this manuscript for commercial applications. All other authors have no conflicts of interest.

Author Manuscript Author Manuscript Author Manuscript Author Manuscript

Abstract

Organ-on-a-chip systems have the potential to revolutionize drug screening and disease modeling through the use of human stem cell-derived cardiomyocytes. The predictive power of these tissue models critically depends on the functional assembly and maturation of human cells that are used as building blocks for organ-on-a-chip systems. To resemble a more adult-like phenotype on these heart-on-a-chip systems, the surrounding micro-environment of individual cardiomyocyte needs to be controlled. Herein, we investigated the impact of four microenvironmental cues: cell seeding density, types and percentages of non-myocyte populations, the types of hydrogels used for tissue inoculation and the electrical conditioning regimes on the structural and functional assembly of human pluripotent stem cell-derived cardiac tissues. Utilizing a novel, plastic and open-access heart-on-a-chip system that is capable of continuous non-invasive monitoring of tissue contractions, we were able to study how different micro-environmental cues affect the assembly of the cardiomyocytes into a functional cardiac tissue. We have defined conditions that resulted in tissues exhibiting hallmarks of the mature human myocardium, such as positive force-frequency relationship and post-rest potentiation.

Graphical Abstract

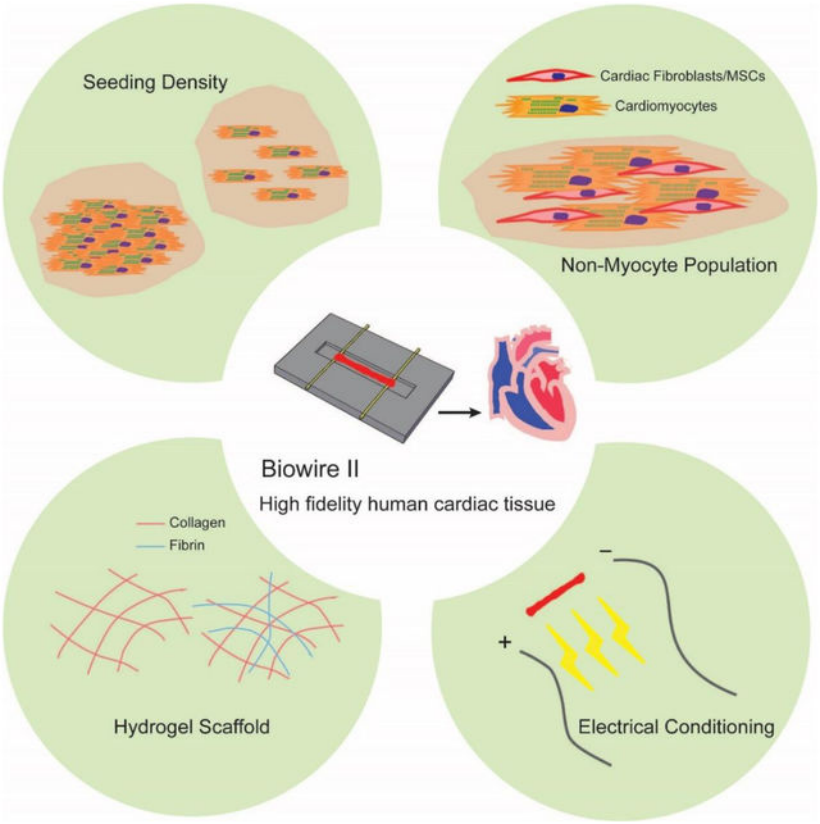

Keywords

cardiomyocytes; tissue engineering; electrophysiology; electrical stimulation; maturation; microenvironment; organ-on-a-chip; heart

Author Manuscript Author Manuscript Author Manuscript Author Manuscript

1. Introduction

Ideally, arrays of functional human 3D cardiac tissues can help eliminate drug candidates with toxicity and delineate the mechanisms of action in the early developmental stages [1, 2]. Differences in cardiac electrophysiology amongst humans and other species, limit the predictive power of current pre-clinical models [3, 4]. Thus this motivates the development of devices that can provide adult-like human myocardium together with the on-line readouts of functional properties such as contraction force. Organ-on-a-chip systems, or more specifically heart-on-a-chip, are becoming increasingly important in pre-clinical drug development. Microenvironmental control is required to create a cardiac tissue on a chip that closely resembles a human myocardium.

In general, three-dimensional micro-tissues have been created through cell-gel compaction in a highly controlled *in vitro* environment, such as cardiac microtissues [5], cardiobundles [6], micro heart muscle [7] and cardiac Biowires [8–10]. In these studies, manipulation of the micro-environment has been used to enhance cardiomyocyte (CM) functional development [8, 11]. For example, cardiac fibroblasts (cFBs) and other stromal cells have been used to promote tissue compaction and remodeling [9, 10, 12]. The total cell seeding density, types and percentages of non-myocytes are important to consider for optimal results, since both CMs that perform the contractile function and non-myocytes such as cFBs that maintain homeostasis of the extracellular matrix are critical elements in healthy native myocardium [9, 10, 12]. Native extracellular proteins and blood-clotting materials such as collagen, Matrigel and fibrin are commonly used scaffolds for cardiac tissue engineering [5, 8, 11]. Although these natural materials yield functional tissues, systematic comparisons in the context of organ-on-a-chip engineering are rarely performed as different research groups tend to use different hydrogels [8, 11].

Electrical stimulation of cardiac tissues was found to be beneficial for improving tissue function and accelerating CM maturation levels. Nunes et al. stepped up electrical pacing frequency from 1 to 3 Hz or from 1 to 6 Hz within a week [8] to enhance the maturation levels of human pluripotent stem cell-derived CMs. Similarly, Ronaldson-Bouchard et al. extended the stimulation period to 3 weeks and reported a more pronounced ventricular maturation [11]. However, results from different studies cannot be compared directly due to the distinct experimental setups used.

Our goal here was to characterize and optimize a user-friendly organ-on-a-chip platform for the cultivation of human pluripotent stem cell-derived cardiac tissues. Unlike common organ-on-a-chip platforms, the described chip is constructed of tissue culture polystyrene and flexible polymer wires that enable on-line tracking of contraction force. The platform, termed Biowire II, has open access for liquid dispensing and enables the creation of cylindrical cardiac microtissues suspended at a constant height. Although there is no microfluidic flow in this system, we consider it to be an organ-on-a-chip device, according to a recent definition [13], since the platform has a significant engineering component and spatially guides cell confinement. Here, we comprehensively explored different culture conditions including seeding density, non-myocyte populations, hydrogel scaffolds and electrical stimulation protocols to define a more controlled seeding and cultivation protocol

Author Manuscript Author Manuscript Author Manuscript Author Manuscript

engineering a mature, functional myocardial tissue that is ideal for drug testing and discovery applications.

2. Results and Discussion

2.1. Biowire II platform enables efficient use of stem cell-derived cardiomyocytes

The Biowire II chip is a strip of patterned tissue culture plastic with eight rectangular microwells for cell seeding and tissue formation (Figure 1). The chip was made of polystyrene, commonly used tissue culture substrate, with two parallel poly(octamethylene maleate (anhydride) citrate) (POMaC) wires affixed at either end of the microwells with a small amount of low absorption adhesive [14]. These wires allow tissues to attach and their displacement is used to estimate passive and active tension generation by the tissues.

The dimensions of the tissue culture microwells (5 mm × 1 mm × 300 μm, L × W × H) were uniquely designed to contain small amounts of cells and facilitate tissue formation. The seeded cells remodel the matrix over the first week of culture, compacting the structure and creating a cylindrical tissue affixed to the polymer wire at each end. As the input cell number increased according to the following groups: 0.05, 0.1, 0.2, 0.3 million cells/tissue by varying the cell seeding density (25, 50, 100, 150 million/mL), we observed that more compaction of the hydrogel by the cells occurred in the 25 and 50 million/mL groups and less in the 100 and 150 million/mL groups (Figure 2A).

To monitor maturation and the quality of our tissues, we measured ET and MCR on day 6 after seeding, at which time the tissues had undergone cell-gel compaction. Tissues in the 25 and 50 million/mL groups had significantly lower ET than the ones in the 100 and 150 million/mL groups (Figure 2B). In addition, 50 million/mL group had significantly higher MCR compared to the 100 million/mL group (Figure 2C).

Tissues from the lowest seeding density exhibited the highest passive tension on day 7 (Figure 2D). After 30 days of culture, passive tension was comparable in all groups (Figure 2E). Active forces were the lowest in 25 million/mL group, which was significantly lower compared to the group of 100 million/mL.

Confocal imaging of GFP labeled CMs, facilitated through the use of HES3-NKX2–$5^{eGFP/w}$ and Vimentin labeled non-cardiomyocyte populations, at day 7 (Figure 2F), enabled us to quantify the cellular alignment of CMs in tissues of various groups (Figure 2G). Quantitative analysis of GFP signal confirmed that groups seeded with 25 and 50 million cells/mL exhibited significantly better cellular alignment in compacted tissues compared to the groups seeded with 100 and 150 million cells/mL (Figure 2G).

Mason’s trichrome staining revealed the more pronounced presence of collagen in the tissues at the lower seeding densities after 30 days of culture (Figure 2H). As expected, the lowest cell density group, the group of 25 million/mL, appeared to be the least cellular, consistent with the lowest active forces. Tissues seeded at a higher density exhibited lower collagen presence, without any visible collagen islands, as more cells can facilitate better remodeling of the collagen hydrogel used for seeding (Figure 2I). More importantly, the

Author Manuscript Author Manuscript Author Manuscript Author Manuscript

yield of cells in the tissue after 30 days of culture was the lowest in the 25 million/mL group, at 31% of the seeded cell number, and comparable in all other groups at 75%~106% of the seeded cell number (Supplemental Figure 1). However, increasing cell number per tissue failed to yield higher active forces, thus motivating the use of lower cell numbers to maintain overall process efficiency.

One of the main goals of this work was to create a tissue with a minimal cell number to facilitate higher throughput studies in drug discovery. Engineered cardiac tissues often require 0.5 – 2 million CMs per tissue [8, 15], motivating the work towards cell number optimization in order to create smaller tissues that require fewer cells, therefore, reducing the overall cost of the preparation and evaluation. We also sought to establish that this platform is effective when using cardiomyocytes derived from several sources (iPSCs and ESCs) as well as to demonstrate the properties of biowires generated from ventricular versus atrial cardiomyocytes derived from these stem cell source. Based on our findings, tissues with a seeding density of 50 million/mL (~0.1 million cells), exhibit better cellular alignment and absence of visible collagen islands, that are characteristic of a healthy myocardium *in vivo*, compared to the 25 million/mL group. In addition, the group seeded with 50 million/mL cells exhibited relatively high active forces throughout the entire culture period, comparable to those generated by seeding 100 and 150 million/mL. Therefore, we have kept our engineer cardiac tissues at a 50 million/mL seeding density to investigate how other micro-environmental cues affect the functional assembly of cardiac tissues.

2.2. Comparison of MSC and cFB as a non-myocyte population

In cardiac tissue engineering, non-myocytes, such as MSCs or cFBs have been commonly added to the engineered ventricular tissues to help with the tissue formation in the short term and remodeling in the long term [8, 11, 16, 17]. As non-contracting and proliferating cells, FBs were considered undesirable during early cardiac tissue engineering studies and were routinely removed by a series of pre-plating steps [18]. Over time tissue engineers learned to harness the power of FBs by introducing them strategically in defined percentages during co-culture with ventricular CMs, to obtain ventricular engineered cardiac tissues with enhanced structural and functional properties and an enhanced ability to survive *in vivo* [19–26]. Alternatively, mesenchymal cell types such as MSCs have also be used [27] to enhance the outcome of ventricular tissue engineering. No differences were observed in the functional outcome when either FBs or MSCs have been used previously in ventricular tissue engineering [27]. In the context of ventricular cardiac tissues based on hESC-derived CMs, we also demonstrated enhanced matrix remodelling and functional properties in cultures with 75% CMs and 25% hESC-derived CD90+ mesodermal cells [26]. Most recent studies describing the generation of atrial tissues used human foreskin [28] or cardiac FBs [29, 30] or no additional non-myocytes [31], thus systematic comparison of FBs to MSC have not been made previously for atrial tissues, motivating our investigation here.

Initially, the compaction of tissues generated with MSCs was delayed compared to tissues with cFBs; however, by day 7 there were no measurable differences between the two sets of tissues (Figure 3A). After day 7, both groups experienced electrical conditioning with an atrial specific protocol (Figure 3B). At the end of cultivation, both tissue types exhibited a

Author Manuscript Author Manuscript Author Manuscript Author Manuscript

densely compacted appearance as shown in Figure 3C. The non-myocyte population did not affect the FFR relationship, as equivalent values (Figure 3D) were obtained. ET and MCR (Figure 3E and F) were improved remarkably with electrical conditioning during culture in both groups, without a significant difference between the MSC and the cFB group at either time point.

The two tissue groups exhibited differences in their action potential profiles (Figure 3G). CMs in the tissues with cFB had a significantly shorter APD_{30} and APD_{50} than the CMs with MSCs, which is a hallmark of functional improvement for atrial CMs (Figure 3H). CMs in the tissues with cFBs had significantly lower amplitude (Figure 3I), less negative minimum diastolic potentials (Figure 3J) and similar upstroke velocity (Figure 3K) compared to the tissues with MSCs.

Cell-mediated compaction of the extracellular matrix (ECM) is a critical modulator in tissue engineering [32], yet different cell types may influence the function of the tissues at the endpoint. Despite both MSCs and cFBs facilitate similar tissue formation, our results indicate that the effect of non-myocytes is more complex in terms of action potential properties. Furthermore, MSCs exhibit plasticity and the extent of integration and coupling to CMs is unknown. By contrast, cFBs exist in native myocardium and are electrically coupled with CMs through gap junctions [33] which has been shown in mathematical modeling studies to modulate the electrical properties of the myocardium [34].

2.3. cFB percentage influences tissue function

In addition to the non-myocyte population type, studies have shown that the percentage of non-myocytes within the microenvironment can also significantly influence the tissue function [26]. Because of the heterogeneous nature of the cell population obtained directly from the ventricular differentiation culture, the CM population ($NKX2.5^+$) was accounted for 76.1±13.0% of total cells on average. The remaining cells were non-myocytes. Here, we compared cardiac tissue function in tissues seeded with either 10% or 25% of additional cFBs in ventricular preparations to facilitate tissue remodeling. Therefore, total non-myocyte population vs. CM was actually equivalent to 3:7 in tissues with 10% additional cFB, i.e. low cFB group, and 4:6 in tissues with 25% additional cFB i.e. high cFB group. The initial 7-day compaction was significantly faster in the high cFB group (Figure 4A and B). After electrical conditioning (Figure 4C), ET and MCR were significantly improved in both groups (Figure 4D and E). Positive FFR is a hallmark of human adult ventricular myocardium, whereas flat FFR is observed in the myocardium of newborns [35]. Recent studies describe the first cultivated engineered cardiac tissue with positive FFR and a remarkable maturation level [11, 36]. Thus, achieving positive FFR became one of the key criteria to evaluate tissue function in our studies.

Here, a positive FFR was achieved for both the low cFB and high cFB group after electrical conditioning (Figure 4F). Importantly, active forces from the low cFB group were significantly higher than those of the high cFB group when paced at the same frequency (Figure 4G) with roughly 3–4 fold difference. This difference in the active force was achieved with the same number of seeded CMs, suggesting that the CMs in the tissues with low cFB have higher efficiency in their contractile machinery likely due to the improved

Author Manuscript Author Manuscript Author Manuscript Author Manuscript

electromechanical connectivity and mechanical coupling. Moreover, tissues from the low cFB group have significantly higher active forces than passive tensions, unlike the opposite trend from high cFB group (Figure 4H). Higher active forces result in higher displacements of the polymer wire, which provides more accurate active force readouts from the platform.

Due to the nature of our system, the tissue experiences higher tension along the longitudinal direction of the microwell during remodeling, which facilitates the uniaxial contraction (Supplemental Figure 2, Supplemental Video 1) [37]. Previous studies suggest that cFBs can sense and align with this tension [38] and therefore facilitate the alignment of CMs. Without adding cFBs to the tissue, the low level of cellular reorganization during the first week led to the formation of a thin film of CM sheet with minimal tissue contraction (Supplemental Figure 3, Supplemental Video 2). Previous studies also show that at low fibroblast density, impulse propagation in cardiac tissues is sustained when CMs couple to more depolarized fibroblasts [39, 40]. In our case, the preferred non-myocyte population is approximately 30% (low cFB group), which is consistent with other studies [26]. However, a further increase in the fibroblast number within the tissue is thought to promote conduction blocks in the areas covered with large fibroblast numbers, thus increasing the tissue stiffness [41] and slowing down conduction [10]. Our results here are consistent with those findings.

2.4. Slower electrical conditioning improves tissue function and consistency

Progressive increase in the frequency of electrical conditioning is proven to be useful for cardiac tissue functional development [8, 11]. Here, we compared two conditioning protocols with different intensity of frequency increase: supra-threshold electrical conditioning of 1Hz weekly step-up and 0.2 Hz daily step-up (Figure 5A). ETs (Figure 5B) were significantly decreased in both groups with electrical conditioning reaching approximately the same levels. MCRs increased after electrical conditioning in both groups. In addition, at the end of electrical conditioning MCR in the 1Hz group was significantly higher than the MCR in the 0.2Hz group (Figure 5C). Similarly, the success rate for tissues to achieve positive FFR were also slightly higher in the 1 Hz than the 0.2 Hz group (Figure 5D). The results were potentially due to the faster overall frequency step-up in 0.2 Hz group (equivalent to 1.4 Hz/week) compared to the 1 Hz group (1Hz/week).

During the frequency ramp-up protocol, conceptually it is important for the tissue to capture the applied pacing frequency. Therefore, slower step-up may be more beneficial. Pronounced positive FFR from 1–3 Hz was observed in both groups without any significant difference (Figure 5E), however, the percent of tissues able to achieve this at the end of the conditioning protocol was lower in the 0.2 Hz group compared to the 1 Hz group, which suggested that 0.2 Hz per day of frequency increase would be too fast for all tissues to achieve desired functional improvement (Figure 5D). Post-rest potentiation (PRP) of force is another hallmark of the adult myocardium in addition to positive FFR. The PRP indicates the capacity of the sarcoplasmic reticulum (SR) in CMs to store, efficiently release and subsequently replenish Ca^{2+}. Both of our stimulation protocols are able to generate tissues with positive FFR. However, tissues from the 1Hz group developed a higher PRP than those of the 0.2 Hz group (Figure 5F). Confocal images of MLC 2v, sarcomeric α-actinin, F-actin, cTNT and Cx43 demonstrated no appreciable differences between the groups (Figure 5G

Author Manuscript Author Manuscript Author Manuscript Author Manuscript

and H). Based on the improvements in the success rate and the functional properties, a weekly 1 Hz step-wise electrical conditioning may be a better approach in further studies.

2.5. Collagen/Fibrin hydrogel blend improves the intracellular organization

In cardiac tissue engineering, hydrogels are primarily used to immobilize cells right after seeding and maximize cardiomyocyte viability by providing structural and mechanical support as well as a biological niche for tissue assembly [42]. Notable recent approaches managed to eliminate the use of hydrogels [7]. However, in our system, the opening of the microwell is too large to enable successful tissue compaction and stabilization in the absence of hydrogels. Here, tissues seeded with Collagen hydrogel or Collagen/Fibrin hydrogel, two commonly used hydrogels in cardiac tissue engineering [5, 43], were compared after conditioning with the 1Hz step-up protocol (Figure 6A). Tissues based on Collagen or a combined Collagen/Fibrin gel developed equivalent ET and MCR (Figure 6B, C). Success rate determined by the percentage of tissues that reached a positive FFR at the end of cultivation, was also equivalent between the two hydrogel groups (Figure 6D).

Pronounced positive FFR and robust PRP were observed in both hydrogel groups without significant differences (Figure 6E, F). Notably, tissues generated with the Collagen/Fibrin hydrogel had more aligned and organized structural proteins, i.e. myosin light chain 2v, sarcomeric α-actinin, F-actin and troponin T, compared to those tissues cultivated from the Collagen hydrogel (Figure 6G, both left and right panel). The myofiber alignment was quantified from confocal images of cTNT staining and a significantly better alignment was shown in Collagen/Fibrin group (Figure 6H). In addition, confocal images of Cx43 staining demonstrated the robust presence of this gap junctional protein in both groups (Figure 6G, right panel).

According to these results, we concluded that both hydrogels were able to serve as a scaffold for tissue formation and maturation. Despite no measurable differences in contractile function, tissues in the Collagen/Fibrin group appeared to have an improved organization of intracellular structural and functional proteins compared to the Collagen only group.

Although collagen and fibrin hydrogels have similar microscopic structures [44], the shear modulus of pure Collagen hydrogel was reported to be only half that of the Collagen/Fibrin hydrogel, according to the studies that used identical Collagen/Fibrin ratio as we have explored here [45]. Lower elastic modulus, higher ultimate tensile stress and toughness were observed in the Collagen/Fibrin gels compared to the pure Collagen gels in the previous studies [46]. In addition, the mechanism of tissue compaction is closely related to cell migration, both of which can be linked to fibrin and its degradation products [47–49]. These differences in chemical and mechanical properties may contribute to better CM alignment and enhanced intracellular organization in the tissues seeded with the fibrin-containing hydrogel.

This study focused on delineating microenvironmental factors governing human cardiac tissue formation in a unique organ-on-a-chip platform that is constructed entirely of cytocompatible low-absorption plastic and enables direct, non-destructive and continuous monitoring of the active force and passive tension of the developing tissue. The optimized

Author Manuscript Author Manuscript Author Manuscript Author Manuscript

microenvironmental factors enabled us to create miniaturized human cardiac tissues with as little as 0.1 million cells, while still obtaining hallmarks of adult-like functionality and maturation such as positive FFR and substantial PRPs. We found that the optimal seeding density for tissue formation was 50 million/mL. As a non-myocyte population for co-culture, cFBs enabled enhancement of electrophysiological properties consistent with cardiac chamber specificity. Further increasing the percentage of added cFBs was found to have detrimental effects on functional properties such as active force. Electrical conditioning was found to consistently enhance structural and functional properties in all groups. Moreover, the slower the frequency step-up, the more cardiac tissues successfully achieved the desired maturity as measured by the tissues ability to achieve a positive FFR. Finally, when comparing hydrogel scaffolds, a collagen hydrogel blended with fibrin enhanced intracellular organization of CMs. Controlling all the micro-environmental cues presented here may give rise to cardiac tissues that have a significant potential to improve the robustness and fidelity of stem cell-derived adult-like cardiac tissue models for use in drug development and disease modelling applications.

3. Experimental Section

3.1. The Fabrication of Biowire Chip

A repeating pattern consisting of rectangular microwells (5 mm × 1 mm × 300 μm, L × W × H) interconnected by two parallel grooves (200 μm × 100 μm, W × H) was designed and fabricated by soft lithography. [50] The negative polydimethylsiloxane (PDMS) master was made by plasma bonding a sheet of patterned PDMS (Mold#1) to a silicon wafer and was used to hot emboss the microwells into a clear polystyrene sheet [16, 51]. Poly(octamethylene maleate (anhydride) citrate) (POMaC) [52] polymer wires (100 μm × 100 μm × 8 cm, W × H × L) were prepared separately. PDMS mold (Mold#2) with channels (100 μm × 100 μm × 8 cm, W × H × L) was lightly pressed against the clean glass slide. The POMaC prepolymer was perfused [16] through the channels and crosslinked with UV exposure. After peeling off the PDMS from the glass slide, POMaC wires were exposed and manually placed into the two parallel grooves patterned into the polystyrene sheet. Approximately 41 mg (after curing) of clear polyurethane 2-part adhesive (SP 1552–2, GS Polymers, Inc.) was used to fix the POMaC wires in place in order to obtain a single strip of 8 microwells [14]. (Figure 1A) The column of eight microwells was cut and used for tissue culture, as shown in the photograph (Figure 1B).

3.2. Cells and Generation of Engineered Cardiac Tissue

Predominantly ventricular cardiomyocytes (CMs) were derived from the human embryonic stem cell (hESC) lines HES3-NKX2–5$^{gfp/w}$ and the human induced pluripotent stem cell (hiPSC) line BJ1D using published differentiation protocols [53, 54]. Ventricular cell populations from BJ1D iPSCs contained 74.7±6.3% (n=9) of CMs, based on cardiac troponin T expression analysis with flow cytometry at day 21 of the differentiation. Ventricular cells from HES3-NKX2.5$^{gfp/w}$ hESCs contained 76.1±13.0% (n=6) CMs, based on GFP+ expression analysis with flow cytometry at day 21 of the differentiation.

Author Manuscript Author Manuscript Author Manuscript Author Manuscript

Predominantly atrial cardiomyocytes were derived from HES3-NKX2–5$^{gfp/w}$ hESCs using an atrial-specific EB differentiation protocol as described [55]. Briefly, all-trans retinoic acid (0.5 μM, Sigma R2625) was added during the cardiac mesoderm specification stage (days 3–5 of differentiation) to promote atrial cardiogenesis. Atrial cardiomyocytes from HES3-NKX2–5$^{gfp/w}$ hESCs were analyzed and defined based on the proportion of NKX2.5+, cTNT+ and MLC2v-cells using flow cytometry on day 20 of differentiation, 79.1±8.0%, n=10. Differentiated cells were dissociated to single cells for subsequent tissue seeding, as previously described [16].

3.3 Flow Cytometry

Cells were obtained by dissociating differentiation cultures with collagenase (200 unit/mL). The cells were fixed with 4% paraformaldehyde (Sigma 158127) in PBS for 10 min at room temperature while shielding from light, to prevent bleaching of GFP fluorescence. For HES3-NKX2–5$^{gfp/w}$ hESC derived ventricular CMs, no further staining was required. For the rest of the cell types, cells were blocked with 5% fetal bovine serum (FBS) (Life Technologies 12483020) in phosphate buffered saline (PBS) for 30 min and followed by permeabilization with PBS containing 5% FBS and 0.1% Triton X (Alfa Aesar A16046) for 10 min on ice. Mouse anti-cardiac Troponin T (cTnT) (ThermoFisher MS295-P; 1:200) and donkey anti-mouse-Alexa Fluor 488 (Abcam ab150105; 1:400) were used subsequently to stain CMs. For HES3-NKX2–5$^{gfp/w}$ hESC derived atrial CMs, additional rabbit anti-myosin light chain-2v (Santa Cruz sc-15370), and Donkey anti-rabbit IgG (H+L), AlexaFluor555 (Thermo Fisher A31572) were used to identify atrial specification.

3.4. Hydrogel Preparation and Seeding Conditions

Collagen hydrogel (0.5mL at 3.0 mg/mL) was prepared with high concentration rat tail collagen (9.82 mg/mL, Corning 354249) with 15 % (v/v) Matrigel (Corning 354230), deionized sterile H_2O and 10 % (v/v) M199 (Sigma M0650) and neutralized by $NaHCO_3$ (E COM SX0320–1) and NaOH (Caledon 7860–1-70). A Collagen/Fibrin hydrogel was prepared by combining the Collagen hydrogel with 33 mg/mL fibrinogen (Sigma-Aldrich F3879) in a 3:1 ratio. When the Collagen/Fibrin hydrogel was used, fibrin conversion to fibrinogen polymer was facilitated by the addition of 0.5 μL of 25 IU/mL thrombin (Sigma-Aldrich) to each well prior to seeding. Aprotinin (10 μM, Sigma A3428) was added in the first week of culture to the media in order to maintain the integrity of fibrin.

For seeding, CMs were dissociated from embryoid bodies or monolayers, they were mixed with the supporting cells, pelleted and resuspended in the specified hydrogel according to the experimental design, then 2 μL of cell-hydrogel mixture was added to each well. In all experiments, the tissues were kept in culture for 7 days to allow for remodeling and compaction around the POMaC wires prior to electrical conditioning.

To optimize seeding density, dissociated cardiac cells (HES3) and cardiac fibroblasts (LONZA, Clonetics™ NHCF-V) were mixed in a 10:2.5 cell number ratio, then they were seeded at four different concentrations: 25, 50, 100, 150 million per mL into the Biowire II wells.

Author Manuscript Author Manuscript Author Manuscript Author Manuscript

Cardiac fibroblasts (cFB) and mesenchymal stem cells (MSC) were compared as non-myocyte populations for atrial tissue formation. Dissociated cardiac cells (HES3) and cFBs or MSC were mixed in 10:1.5 cell number ratios respectively.

To determine the appropriate fraction of non-myocytes, dissociated cardiac cells (HES3) and cardiac fibroblasts were mixed in 10:1 and 10:2.5 cell number ratios, for low cFB and high cFB groups respectively.

For hydrogel optimization, dissociated cardiac cells (BJ1D) and cFBs were mixed in 10:1 cell number ratio, in collagen hydrogel or collagen/fibrin hydrogel at 50 million per mL.

For electrical conditioning optimization, dissociated cardiac cells (BJ1D) and cFBs were mixed in 10:1 cell number ratio, in collagen hydrogel at 50 million per mL.

3.5. Electrical Stimulation

On day 7, tissues were transferred to an electrical stimulation chamber, as previously described [29], for electrical conditioning. Briefly, for ventricular tissues frequency was ramped up by 1Hz per week from 2 Hz to 6 Hz unless otherwise specified. For the optimization of electrical conditioning, two protocols were compared: 1Hz weekly increase from 2–6 Hz and 0.2 Hz daily increase from 1–6 Hz. For atrial preparations, the frequency was increased daily by 0.4 Hz, from 2 Hz to 6 Hz, then retained at 6 Hz for 1week.

3.6. Evaluation of Active Force and Passive Tension

POMaC wires have an intrinsic autofluorescence in the blue channel, enabling us to determine wire deflection from the movies of tissue contraction taken in the blue channel (10X objective; λ_{ex} = 350 nm, λ_{em} = 470 nm; 100 frames/s, 5 ms exposure). To determine the force-frequency relationship (FFR), the tissues were electrically paced from 1–6 Hz (20 sec/each frequency). After the last period of high-frequency pacing, a short period of rest was induced by turning the stimulator off, followed by reinitiation of pacing at 1 Hz to determine post-rest potentiation (PRP). All imaging was performed by Olympus IX81 inverted fluorescent microscope and CellSens software (Olympus Corporation)

Sequential images from the blue channel recording were analyzed using a custom MatLab code that traced the maximum deflection of the POMaC wire. Total (at peak contraction) and passive (at rest) POMaC wire deflections were converted to force measurements (μN) using the force calibration curves described elsewhere.[56] The active force was calculated as the difference between the total and passive tension. The custom MatLab code was used to calculate the passive tension, active force, contraction and relaxation duration, and upstroke and relaxation velocity.[56]

3.7. Immunostaining, Confocal Microscopy and Myofiber Alignment Quantification.

Tissues were fixed with 4% paraformaldehyde, permeabilized with 0.2% Tween20, and blocked with 10% fetal bovine serum (FBS). The following primary antibodies were used: mouse anti-cardiac Troponin T (cTnT) (ThermoFisher MS295-P; 1:200), rabbit anti-Connexin 43 (Cx-43) (Abcam ab11370; 1:200), mouse anti-α-actinin (Abcam ab9465; 1:200), rabbit anti-myosin light chain-2v (Santa Cruz ab9465; 1:200). The following

Author Manuscript Author Manuscript Author Manuscript Author Manuscript

secondary antibodies were used: donkey anti-mouse-Alexa Fluor 488 (Abcam ab150105; 1:400) and donkey anti-rabbit-Alexa Fluor 594 (Abcam ab150080; 1:200). Phalloidin-Alexa Fluor 660 (Invitrogen A22285; 1:200) was used to stain F-actin fibers. Conjugated vimentin-Cy3 (Sigma C9080; 1:200) was used to stain for vimentin. Confocal microscopy images were obtained using an Olympus FluoView 1000 laser scanning confocal microscope (Olympus Corporation).

The alignment ratio was calculated using ImageJ plugin OrientationJ (Biomedical Imaging Group). The distribution analysis was performed using a Gaussian filter with a window of 2 pixels (cTNT) and 10 pixels (GFP^+).[57]

3.8. Brightfield Images from Histological Staining and the Quantification of Collagen

Paraffin-embedded tissues were sectioned at 5μm thickness. Masson's trichrome staining was then performed to reveal the collagen fibers, cells and cell nuclei followed by brightfield imaging on Olympus IX81 inverted microscope.

Area of collagen staining was determined by ImageJ color threshold analysis with Blue (0–255), green (180–255) and red (120–210). The total area of tissue was determined by manually tracing the tissue edges and measuring pixel numbers in the enclosed area.

3.9 Determination of Excitation Threshold and Maximum Capture Rate

Excitation Threshold (ET) and Maximum Capture Rate (MCR) of tissues were measured in the stimulation chamber connected to an electrical stimulator (S88x Stimulator, GRASS, Astromed). The tissues in the stimulation chamber were placed in a preconditioned environmental chamber (37°C and 5% CO_2). The beating of the tissues was monitored under brightfield with electrical pacing. To find ET, the frequency and the duration of the monophasic electrical pulses were set to 1Hz and 2ms, respectively. The minimum voltage needed to induce the synchronous contraction of the tissue, i.e. ET, was tested by starting from 1 V/cm and increasing the stimulation amplitude in increments of 0.1 V/cm until the synchrony of tissue contraction was achieved. To find MCR, the voltage was set to twice the average ET for all tissues in the stimulation chamber. The maximum frequency allowing synchronous contraction, i.e. MCR, was found by increasing the stimulation frequency in 0.1 Hz increments starting from 1 Hz until the synchrony of tissue contraction was clearly interrupted.

3.10. Intracellular Recordings

Tissues were perfused with 35–37 °C Kreb's Solution (Sigma K4002) (118 mM NaCl, 4.2 mM KCl, 1.2 mM KH_2PO_4, 1.2 mM $MgSO_4$, 1.8 mM $CaCl_2$, 23 mM $NaHCO_3$, 2 mM Na-pyruvate and 20 mM glucose, equilibrated with 95% O_2 and 5% CO_2; pH 7.4). They were paced at twice the ET. The action potential was recorded with high impedance microelectrodes (60–90 MΩ) filled with 3 M KCl, connected to an Axopatch 200 B amplifier (Axon Instruments). Recordings were performed in current clamp mode at 10 kHz by clampex 10 and signals were analyzed using the Clampfit 10 Data Analysis Module of the pCLAMP™ 10 Electrophysiology Data Acquisition & Analysis Software (Axon

Author Manuscript Author Manuscript Author Manuscript Author Manuscript

Instruments). The movement of the tissue was minimized by perfusing with 10μM blebbistatin (Toronto Research Chemicals) for 20min.

3.11. DNA quantification

Tissues were harvested from the Biowire II platform to estimate the total number of cells from each tissue after 30 days of culture. The tissues were lysed with 1X cell lysis buffer (Cell Signalling 9803) for 1 h in room temperature and then homogenized with the ultra-sonicator for 2 seconds. The supernatant was collected and analyzed with Quant-iT PicoGreen dsDNA Assay Kit (Thermo Fisher P11496) according to the manufacturer's protocol. The fluorescent nucleic acid signal from each cardiac tissue was correlated to a standard curve generated by extracting and measuring DNA from a known number of cardiac cells.

3.12. Statistics

Statistical analysis was performed using Prism 6.0 and SigmaPlot 12.0. All data are represented as mean ± standard derivation (SD). Indicated sample sizes (n) represent individual tissue samples. For intracellular recordings, sample size (n) represents the number of cells analyzed from three or more independent experiments. Differences between experimental groups were analyzed by Student's t-test or Mann-Whitney test or one-way ANOVA or ANOVA on ranks. Experiments with two different variables were analyzed with two-way ANOVA. Holm-Sidak and Tukey's multiple comparison methods were used with one-way and two-way ANOVA. Dunn's multiple comparison method was used with ANOVA on ranks. $P<0.05$ was considered significant for all statistical tests.

Supplementary Material

Refer to Web version on PubMed Central for supplementary material.

Acknowledgments:

Grants: This work was funded by the Canadian Institutes of Health Research (CIHR) Operating Grants (MOP-126027 and MOP-137107), Nature Sciences and Engineering Research Council of Canada (NSERC) Discovery Grant (RGPIN 326982–10), NSERC-CIHR Collaborative Health Research Grant (CHRP 493737–16) and National Institutes of Health Grant 2R01 HL076485. MR was supported by NSERC Steacie Fellowship and Canada Research Chair. YZ was supported by NSERC Post-graduate Fellowship, NSERC CREATE Toep student award and Ted Rogers Center for Heart Research Doctoral Award.

The authors would like to acknowledge the help of Stasja Drecun, Seung Doo (Charlie) Yang and Friday Anighoro with data analysis. Dr. Iran Rashedi and Dr. Armand Keating for a kind gift of MSCs.

4. References

[1]. Zhao Y, Korolj A, Feric N, Radisic M, Human pluripotent stem cell-derived cardiomyocyte based models for cardiotoxicity and drug discovery, Expert opinion on drug safety 15(11) (2016) 1455–1458. [PubMed: 27560951]

[2]. Zhao Y, Feric NT, Thavandiran N, Nunes SS, Radisic M, The role of tissue engineering and biomaterials in cardiac regenerative medicine, The Canadian journal of cardiology 30(11) (2014) 1307–22. [PubMed: 25442432]

[3]. Gintant G, Sager PT, Stockbridge N, Evolution of strategies to improve preclinical cardiac safety testing, Nature reviews. Drug discovery 15(7) (2016) 457–71. [PubMed: 26893184]

Author Manuscript Author Manuscript Author Manuscript Author Manuscript

[4]. Sala L, Bellin M, Mummery CL, Integrating cardiomyocytes from human pluripotent stem cells in safety pharmacology: has the time come?, British journal of pharmacology (2016).

[5]. Boudou T, Legant WR, Mu A, Borochin MA, Thavandiran N, Radisic M, Zandstra PW, Epstein JA, Margulies KB, Chen CS, A microfabricated platform to measure and manipulate the mechanics of engineered cardiac microtissues, Tissue engineering. Part A 18(9–10) (2012) 910–9. [PubMed: 22092279]

[6]. Jackman CP, Carlson AL, Bursac N, Dynamic culture yields engineered myocardium with near-adult functional output, Biomaterials 111 (2016) 66–79. [PubMed: 27723557]

[7]. Huebsch N, Loskill P, Deveshwar N, Spencer CI, Judge LM, Mandegar MA, Fox CB, Mohamed TM, Ma Z, Mathur A, Sheehan AM, Truong A, Saxton M, Yoo J, Srivastava D, Desai TA, So PL, Healy KE, Conklin BR, Miniaturized iPS-Cell-Derived Cardiac Muscles for Physiologically Relevant Drug Response Analyses, Scientific reports 6 (2016) 24726. [PubMed: 27095412]

[8]. Nunes SS, Miklas JW, Liu J, Aschar-Sobbi R, Xiao Y, Zhang B, Jiang J, Masse S, Gagliardi M, Hsieh A, Thavandiran N, Laflamme MA, Nanthakumar K, Gross GJ, Backx PH, Keller G, Radisic M, Biowire: a platform for maturation of human pluripotent stem cell-derived cardiomyocytes, Nature methods 10(8) (2013) 781–7. [PubMed: 23793239]

[9]. Nattel S, Electrical coupling between cardiomyocytes and fibroblasts: experimental testing of a challenging and important concept, Cardiovascular research 114(3) (2018) 349–352. [PubMed: 29360945]

[10]. Sachse FB, Moreno AP, Abildskov JA, Electrophysiological modeling of fibroblasts and their interaction with myocytes, Annals of biomedical engineering 36(1) (2008) 41–56. [PubMed: 17999190]

[11]. Ronaldson-Bouchard K, Ma SP, Yeager K, Chen T, Song L, Sirabella D, Morikawa K, Teles D, Yazawa M, Vunjak-Novakovic G, Advanced maturation of human cardiac tissue grown from pluripotent stem cells, Nature 556(7700) (2018) 239–243. [PubMed: 29618819]

[12]. Singh A, Singh A, Sen D, Mesenchymal stem cells in cardiac regeneration: a detailed progress report of the last 6 years (2010–2015), Stem cell research & therapy 7(1) (2016) 82. [PubMed: 27259550]

[13]. Zhang B, Korolj A, Lai BFL, Radisic M, Advances in organ-on-a-chip engineering, Nature Reviews Materials 3(8) (2018) 257–278.

[14]. Domansky K, Leslie DC, McKinney J, Fraser JP, Sliz JD, Hamkins-Indik T, Hamilton GA, Bahinski A, Ingber DE, Clear castable polyurethane elastomer for fabrication of microfluidic devices, Lab on a chip 13(19) (2013) 3956–64. [PubMed: 23954953]

[15]. Mannhardt I, Breckwoldt K, Letuffe-Breniere D, Schaaf S, Schulz H, Neuber C, Benzin A, Werner T, Eder A, Schulze T, Klampe B, Christ T, Hirt MN, Huebner N, Moretti A, Eschenhagen T, Hansen A, Human Engineered Heart Tissue: Analysis of Contractile Force, Stem cell reports 7(1) (2016) 29–42. [PubMed: 27211213]

[16]. Zhang B, Montgomery M, Chamberlain MD, Ogawa S, Korolj A, Pahnke A, Wells LA, Masse S, Kim J, Reis L, Momen A, Nunes SS, Wheeler AR, Nanthakumar K, Keller G, Sefton MV, Radisic M, Biodegradable scaffold with built-in vasculature for organ-on-a-chip engineering and direct surgical anastomosis, Nature materials 15(6) (2016) 669–78. [PubMed: 26950595]

[17]. Rashedi I, Talele N, Wang XH, Hinz B, Radisic M, Keating A, Collagen scaffold enhances the regenerative properties of mesenchymal stromal cells, PloS one 12(10) (2017) e0187348. [PubMed: 29088264]

[18]. Bursac N, Papadaki M, Cohen RJ, Schoen FJ, Eisenberg SR, Carrier R, Vunjak-Novakovic G, Freed LE, Cardiac muscle tissue engineering: toward an in vitro model for electrophysiological studies, The American journal of physiology 277(2) (1999) H433–44. [PubMed: 10444466]

[19]. Caspi O, Lesman A, Basevitch Y, Gepstein A, Arbel G, Habib IH, Gepstein L, Levenberg S, Tissue engineering of vascularized cardiac muscle from human embryonic stem cells, Circulation research 100(2) (2007) 263–72. [PubMed: 17218605]

[20]. Lesman A, Habib M, Caspi O, Gepstein A, Arbel G, Levenberg S, Gepstein L, Transplantation of a tissue-engineered human vascularized cardiac muscle, Tissue engineering. Part A 16(1) (2010) 115–25. [PubMed: 19642856]

Author Manuscript Author Manuscript Author Manuscript Author Manuscript

[21]. Iyer RK, Chiu LL, Radisic M, Microfabricated poly(ethylene glycol) templates enable rapid screening of triculture conditions for cardiac tissue engineering, Journal of biomedical materials research. Part A 89(3) (2009) 616–31. [PubMed: 18442120]

[22]. Iyer RK, Chiu LL, Vunjak-Novakovic G, Radisic M, Biofabrication enables efficient interrogation and optimization of sequential culture of endothelial cells, fibroblasts and cardiomyocytes for formation of vascular cords in cardiac tissue engineering, Biofabrication 4(3) (2012) 035002. [PubMed: 22846187]

[23]. Iyer RK, Odedra D, Chiu LL, Vunjak-Novakovic G, Radisic M, VEGF Secretion by Non-Myocytes Modulates Connexin-43 Levels in Cardiac Organoids, Tissue engineering. Part A (2012).

[24]. Naito H, Melnychenko I, Didie M, Schneiderbanger K, Schubert P, Rosenkranz S, Eschenhagen T, Zimmermann WH, Optimizing engineered heart tissue for therapeutic applications as surrogate heart muscle, Circulation 114(1 Suppl) (2006) I72–8. [PubMed: 16820649]

[25]. Stevens KR, Kreutziger KL, Dupras SK, Korte FS, Regnier M, Muskheli V, Nourse MB, Bendixen K, Reinecke H, Murry CE, Physiological function and transplantation of scaffold-free and vascularized human cardiac muscle tissue, Proceedings of the National Academy of Sciences of the United States of America 106(39) (2009) 16568–73. [PubMed: 19805339]

[26]. Thavandiran N, Dubois N, Mikryukov A, Masse S, Beca B, Simmons CA, Deshpande VS, McGarry JP, Chen CS, Nanthakumar K, Keller GM, Radisic M, Zandstra PW, Design and formulation of functional pluripotent stem cell-derived cardiac microtissues, Proceedings of the National Academy of Sciences of the United States of America 110(49) (2013) E4698–707. [PubMed: 24255110]

[27]. Tulloch NL, Muskheli V, Razumova MV, Korte FS, Regnier M, Hauch KD, Pabon L, Reinecke H, Murry CE, Growth of engineered human myocardium with mechanical loading and vascular coculture, Circulation research 109(1) (2011) 47–59. [PubMed: 21597009]

[28]. Cyganek L, Tiburcy M, Sekeres K, Gerstenberg K, Bohnenberger H, Lenz C, Henze S, Stauske M, Salinas G, Zimmermann WH, Hasenfuss G, Guan K, Deep phenotyping of human induced pluripotent stem cell-derived atrial and ventricular cardiomyocytes, JCI insight 3(12) (2018).

[29]. Zhao Y, Rafatian N, Feric NT, Cox BJ, Aschar-Sobbi R, Wang EY, Aggarwal P, Zhang B, Conant G, Ronaldson-Bouchard K, Pahnke A, Protze S, Lee JH, Davenport Huyer L, Jekic D, Wickeler A, Naguib HE, Keller GM, Vunjak-Novakovic G, Broeckel U, Backx PH, Radisic M, A Platform for Generation of Chamber-Specific Cardiac Tissues and Disease Modeling, Cell 176(4) (2019) 913–927 e18. [PubMed: 30686581]

[30]. Zhao Y, Rafatian N, Feric NT, Cox B, Aschar-Sobbi R, Wang EY, Aggarwal P, Zhang B, Conant G, Ronaldson-Bouchard K, Pahnke A, Protze S, Lee JH, Davenport Huyer L, Jekic D, Wickeler A, Naguib H, Keller GM, Vunjak-Novakovic G, Broeckel U, Backx PH, Radisic M, A platform for generation of chamber specific cardiac tissues and disease modelling, Cell in press (2018).

[31]. Lemme M, Ulmer BM, Lemoine MD, Zech ATL, Flenner F, Ravens U, Reichenspurner H, Rol-Garcia M, Smith G, Hansen A, Christ T, Eschenhagen T, Atrial-like Engineered Heart Tissue: An In Vitro Model of the Human Atrium, Stem cell reports 11(6) (2018) 1378–1390. [PubMed: 30416051]

[32]. Bell E, Ehrlich HP, Buttle DJ, Nakatsuji T, Living tissue formed in vitro and accepted as skin-equivalent tissue of full thickness, Science 211(4486) (1981) 1052–4. [PubMed: 7008197]

[33]. Vasquez C, Benamer N, Morley GE, The cardiac fibroblast: functional and electrophysiological considerations in healthy and diseased hearts, Journal of cardiovascular pharmacology 57(4) (2011) 380–8. [PubMed: 21242811]

[34]. Maleckar MM, Greenstein JL, Giles WR, Trayanova NA, Electrotonic Coupling between Human Atrial Myocytes and Fibroblasts Alters Myocyte Excitability and Repolarization, Biophysical journal 97(8) (2009) 2179–2190. [PubMed: 19843450]

[35]. Wiegerinck RF, Cojoc A, Zeidenweber CM, Ding G, Shen M, Joyner RW, Fernandez JD, Kanter KR, Kirshbom PM, Kogon BE, Wagner MB, Force frequency relationship of the human ventricle increases during early postnatal development, Pediatric research 65(4) (2009) 414–9. [PubMed: 19127223]

[36]. Tiburcy M, Hudson JE, Balfanz P, Schlick S, Meyer T, Chang Liao ML, Levent E, Raad F, Zeidler S, Wingender E, Riegler J, Wang M, Gold JD, Kehat I, Wettwer E, Ravens U, Dierickx P,

Author Manuscript Author Manuscript Author Manuscript Author Manuscript

van Laake LW, Goumans MJ, Khadjeh S, Toischer K, Hasenfuss G, Couture LA, Unger A, Linke WA, Araki T, Neel B, Keller G, Gepstein L, Wu JC, Zimmermann WH, Defined Engineered Human Myocardium With Advanced Maturation for Applications in Heart Failure Modeling and Repair, Circulation 135(19) (2017) 1832–1847. [PubMed: 28167635]

[37]. Rhee S, Fibroblasts in three dimensional matrices: cell migration and matrix remodeling, Exp Mol Med 41(12) (2009) 858–865. [PubMed: 19745603]

[38]. Tomasek JJ, Gabbiani G, Hinz B, Chaponnier C, Brown RA, Myofibroblasts and mechano-regulation of connective tissue remodelling, Nat Rev Mol Cell Bio 3(5) (2002) 349–363. [PubMed: 11988769]

[39]. Xie Y, Garfinkel A, Camelliti P, Kohl P, Weiss JN, Qu Z, Effects of fibroblast-myocyte coupling on cardiac conduction and vulnerability to reentry: A computational study, Heart rhythm : the official journal of the Heart Rhythm Society 6(11) (2009) 1641–9.

[40]. Jacquemet V, Henriquez CS, Loading effect of fibroblast-myocyte coupling on resting potential, impulse propagation, and repolarization: insights from a microstructure model, American journal of physiology. Heart and circulatory physiology 294(5) (2008) H2040–52. [PubMed: 18310514]

[41]. Herum KM, Lunde IG, McCulloch AD, Christensen G, The Soft-and Hard-Heartedness of Cardiac Fibroblasts: Mechanotransduction Signaling Pathways in Fibrosis of the Heart, J Clin Med 6(5) (2017).

[42]. K. NJ, K. RJ, M. AJ, Coulombe KLK, Optimizing Blended Collagen-Fibrin Hydrogels for Cardiac Tissue Engineering with Human iPSC-derived Cardiomyocytes, ACS Biomaterials Science & Engineering DOI: 10.1021/acsbiomaterials.8b01112 (2018).

[43]. Schaaf S, Shibamiya A, Mewe M, Eder A, Stohr A, Hirt MN, Rau T, Zimmermann WH, Conradi L, Eschenhagen T, Hansen A, Human engineered heart tissue as a versatile tool in basic research and preclinical toxicology, PloS one 6(10) (2011) e26397. [PubMed: 22028871]

[44]. Lai VK, Lake SP, Frey CR, Tranquillo RT, Barocas VH, Mechanical behavior of collagen-fibrin co-gels reflects transition from series to parallel interactions with increasing collagen content, Journal of biomechanical engineering 134(1) (2012) 011004. [PubMed: 22482659]

[45]. Kong YP, Carrion B, Singh RK, Putnam AJ, Matrix identity and tractional forces influence indirect cardiac reprogramming, Scientific reports 3 (2013) 3474. [PubMed: 24326998]

[46]. Cummings CL, Gawlitta D, Nerem RM, Stegemann JP, Properties of engineered vascular constructs made from collagen, fibrin, and collagen-fibrin mixtures, Biomaterials 25(17) (2004) 3699–706. [PubMed: 15020145]

[47]. Nomura H, Naito M, Iguchi A, Thompson WD, Smith EB, Fibrin gel induces the migration of smooth muscle cells from rabbit aortic explants, Thrombosis and haemostasis 82(4) (1999) 1347–52. [PubMed: 10544926]

[48]. Sporn LA, Bunce LA, Francis CW, Cell proliferation on fibrin: modulation by fibrinopeptide cleavage, Blood 86(5) (1995) 1802–10. [PubMed: 7655010]

[49]. Neidert MR, Lee ES, Oegema TR, Tranquillo RT, Enhanced fibrin remodeling in vitro with TGF-beta1, insulin and plasmin for improved tissue-equivalents, Biomaterials 23(17) (2002) 3717–31. [PubMed: 12109697]

[50]. Martin C, Sofla A, Zhang BY, Nunes SS, Radisic M, Fusible core molding for the fabrication of branched, perfusable, three-dimensional microvessels for vascular tissue engineering, Int J Artif Organs 36(3) (2013) 159–165. [PubMed: 23404637]

[51]. Zhao Y, Wang EY, Davenport LH, Liao Y, Yeager K, Vunjak-Novakovic G, Radisic M, Zhang B, A Multimaterial Microphysiological Platform Enabled by Rapid Casting of Elastic Microwires, Advanced healthcare materials (2019) e1801187. [PubMed: 30737909]

[52]. Tran RT, Thevenot P, Gyawali D, Chiao JC, Tang L, Yang J, Synthesis and characterization of a biodegradable elastomer featuring a dual crosslinking mechanism, Soft matter 6(11) (2010) 2449–2461. [PubMed: 22162975]

[53]. Lian X, Hsiao C, Wilson G, Zhu K, Hazeltine LB, Azarin SM, Raval KK, Zhang J, Kamp TJ, Palecek SP, Robust cardiomyocyte differentiation from human pluripotent stem cells via temporal modulation of canonical Wnt signaling, Proceedings of the National Academy of Sciences of the United States of America 109(27) (2012) E1848–57. [PubMed: 22645348]

Author Manuscript Author Manuscript Author Manuscript Author Manuscript

[54]. Lian X, Zhang J, Azarin SM, Zhu K, Hazeltine LB, Bao X, Hsiao C, Kamp TJ, Palecek SP, Directed cardiomyocyte differentiation from human pluripotent stem cells by modulating Wnt/beta-catenin signaling under fully defined conditions, Nature protocols 8(1) (2013) 162–75. [PubMed: 23257984]

[55]. Lee JH, Protze SI, Laksman Z, Backx PH, Keller GM, Human Pluripotent Stem Cell-Derived Atrial and Ventricular Cardiomyocytes Develop from Distinct Mesoderm Populations, Cell stem cell 21(2) (2017) 179–194 e4. [PubMed: 28777944]

[56]. Zhao Y, Rafatian N, Feric N, Cox B, Aschar-Sobbi R, Wang Y, Aggarwal P, Zhang B, Conant G, Ronaldson-Bouchard K, Pahnke A, Protze S, Lee JH, Davenport Huyer L, Jekic D, Wickeler A, Naguib H, Keller G, Vunjak-Novakovic G, Broeckel U, B. P, Radisic M, A platform for generation of chamber specific cardiac tissues and disease modeling, Cell (2018).

[57]. Nunes SS, Feric N, Pahnke A, Miklas JW, Li M, Coles J, Gagliardi M, Keller G, Radisic M, Human Stem Cell-Derived Cardiac Model of Chronic Drug Exposure, ACS Biomaterials Science & Engineering 3(9) (2017) 11.

Author Manuscript Author Manuscript Author Manuscript Author Manuscript

Highlights:

- A brand new, plastic, heart-on-a-chip platform capable of continuous non-invasive monitoring of the active force and passive tension.
- Defined conditions that result in tissues exhibiting positive force-frequency relationship and post-rest potentiation, hallmarks of the mature human myocardium.
- Intermediate seeding density results in a highly aligned cardiac tissue with minimal cell input.
- Cardiac fibroblasts and mesenchymal stem cells are equally effective as a supporting cell population for cardiac tissue formation.
- Higher percentage of added cardiac fibroblasts hinders functional properties.
- Slower ramp-up of frequency of electrical conditioning (1Hz/week) is more beneficial than a faster ramp-up (0.2Hz/day).
- Fibrin hydrogel enhances cardiac structure in organ-on-a-chip platform compared to the collagen hydrogel.

Author Manuscript Author Manuscript Author Manuscript Author Manuscript

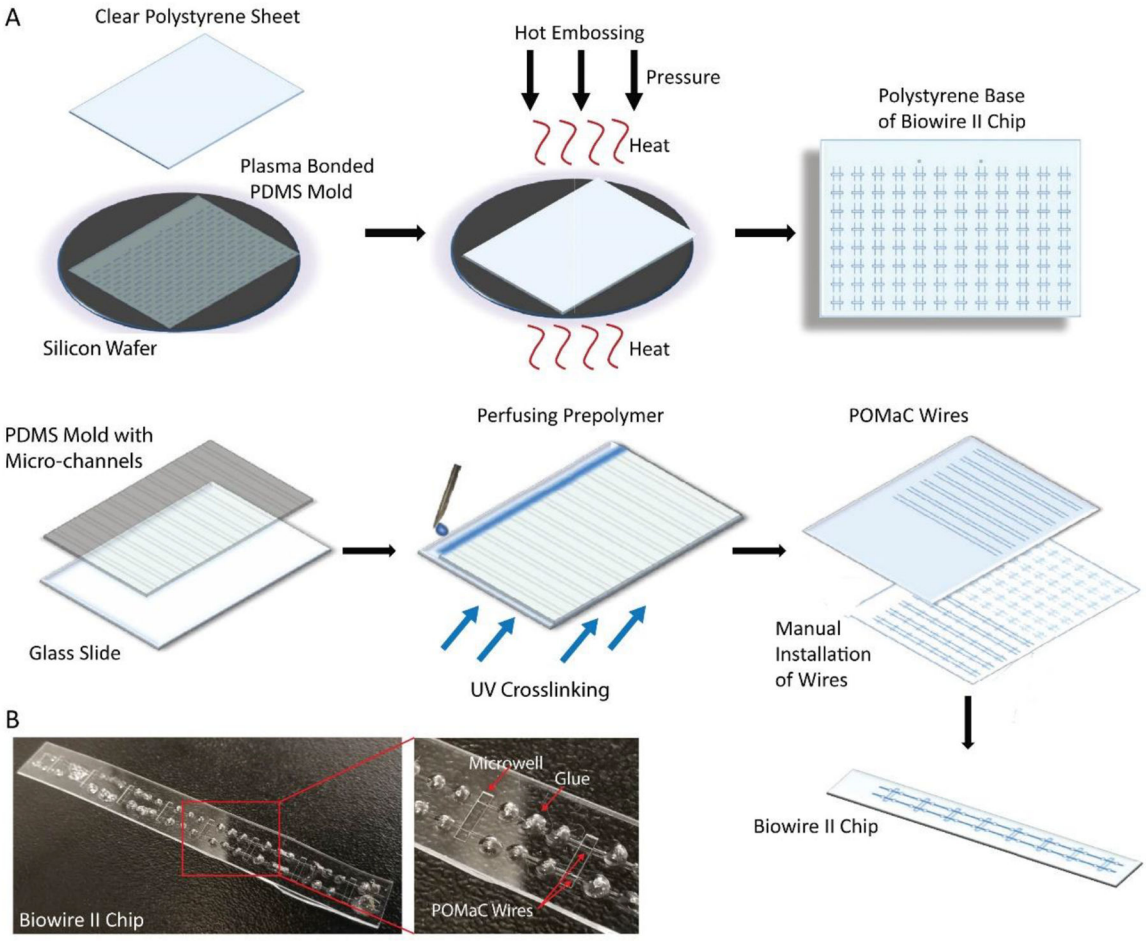

Figure 1: Schematic of the fabrication of the Biowire II Platform.

A) A polydimethylsiloxane (PDMS) mold was cast from an SU-8 master mold prepared with the desired microwell and groove topography. The PDMS mold was plasma bonded to a silicon wafer. A clear polystyrene sheet was placed on top of the bonded wafer and hot embossed using optimized heat and pressure under vacuum. After cooling, the polystyrene sheet imprinted with microwells and grooves, was separated from the PDMS mold. A second PDMS mold with a series of parallel microchannels was cast and perfused with POMaC prepolymer to form the polymer wires. After crosslinking under UV light, the POMaC wires were manually placed into the grooves on the polystyrene base. Polyurethane glue was used to fix the POMaC wires in place. The polystyrene sheet was then cut into columns of 8 microwells. B) Photograph of a single Biowire II strip after fabrication.

Author Manuscript Author Manuscript Author Manuscript Author Manuscript

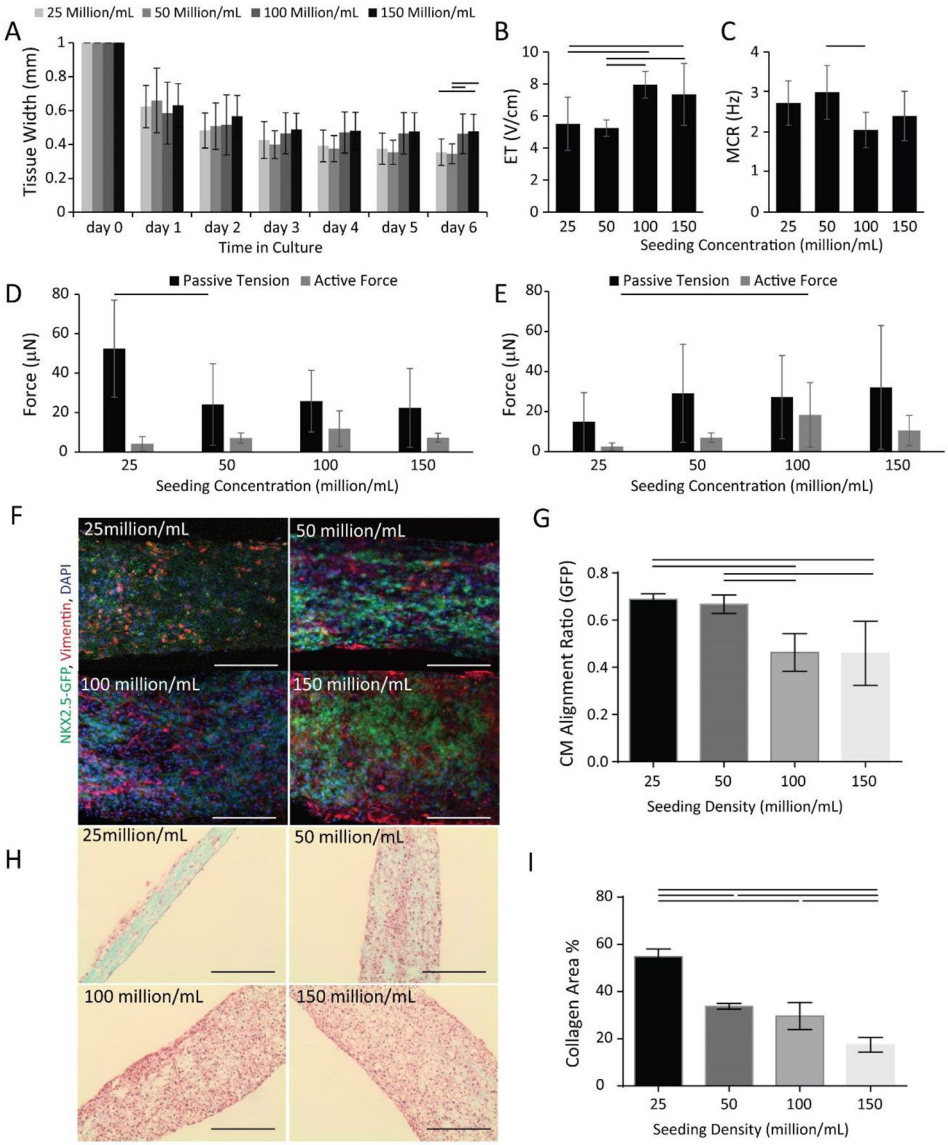

Figure 2: Cell seeding density influences cardiac tissue structure and function in the Biowire II platform.

HES3 ESC derived ventricular tissues were seeded using collagen hydrogel at the concentration of 25, 50, 100, 150 million cells per mL. A) Tissue compaction; B) Excitation threshold (ET) and C) Maximum capture rate (MCR) at day 7. (n⩾8) Active force and passive tension, at D) day 7 (n⩾6) and E) day 30 (n⩾5) of culture were examined. F) Confocal images of NKX2.5-GFP (green) and Vimentin (red) with DAPI (blue) nuclear counterstaining at day 7, (n⩾3), scale bar=100 μm. G) Quantification of CM alignment based on the GFP signal. H) Bright field images of tissues stained by Masson's Trichrome after 30 days of culture, scale bar = 200 μm. I) Quantification of collagen area, (n⩾3). Data are presented as mean ± stdev, one-way ANOVA with Holm-Sidak's multiple comparison test or ANOVA on ranks with Dunn's method.

Author Manuscript Author Manuscript Author Manuscript Author Manuscript

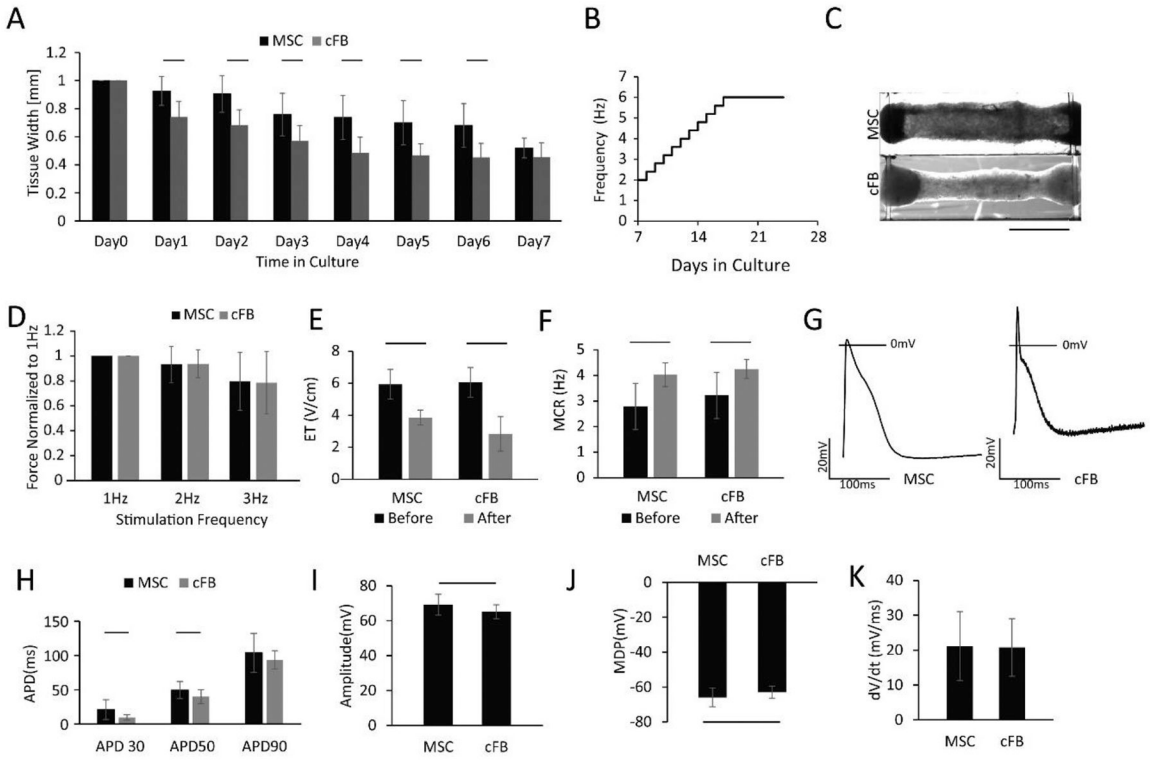

Figure 3: Comparison of non-myocyte populations, mesenchymal stem cells (MSC) and cardiac fibroblasts (cFB), in Biowire II platform.

A) HES3 ESC derived atrial tissues compacted during the first week of culture. (n⩾10) B) Atrial specific electrical conditioning protocol. C) Tissue appearance at the endpoint of culture after electrical conditioning. D) Force-frequency relationship (FFR) (n⩾15). E) Excitation threshold (ET) and F) Maximum capture rate (MCR) were significantly improved after electrical conditioning in both groups. (n⩾10) G) Action potential profiles, H) action potential duration, I) action potential amplitude, J) minimum diastolic potential and K) upstroke velocity were compared between the tissues with the two cell types. For electrophysiological assessment, the AP parameters were multiple pokes from at least three tissues. Data presented as mean ± stdev, Student's t-test or Mann-Whitney test or ANOVA on ranks with Dunn's multiple comparisons test.

Author Manuscript Author Manuscript Author Manuscript Author Manuscript

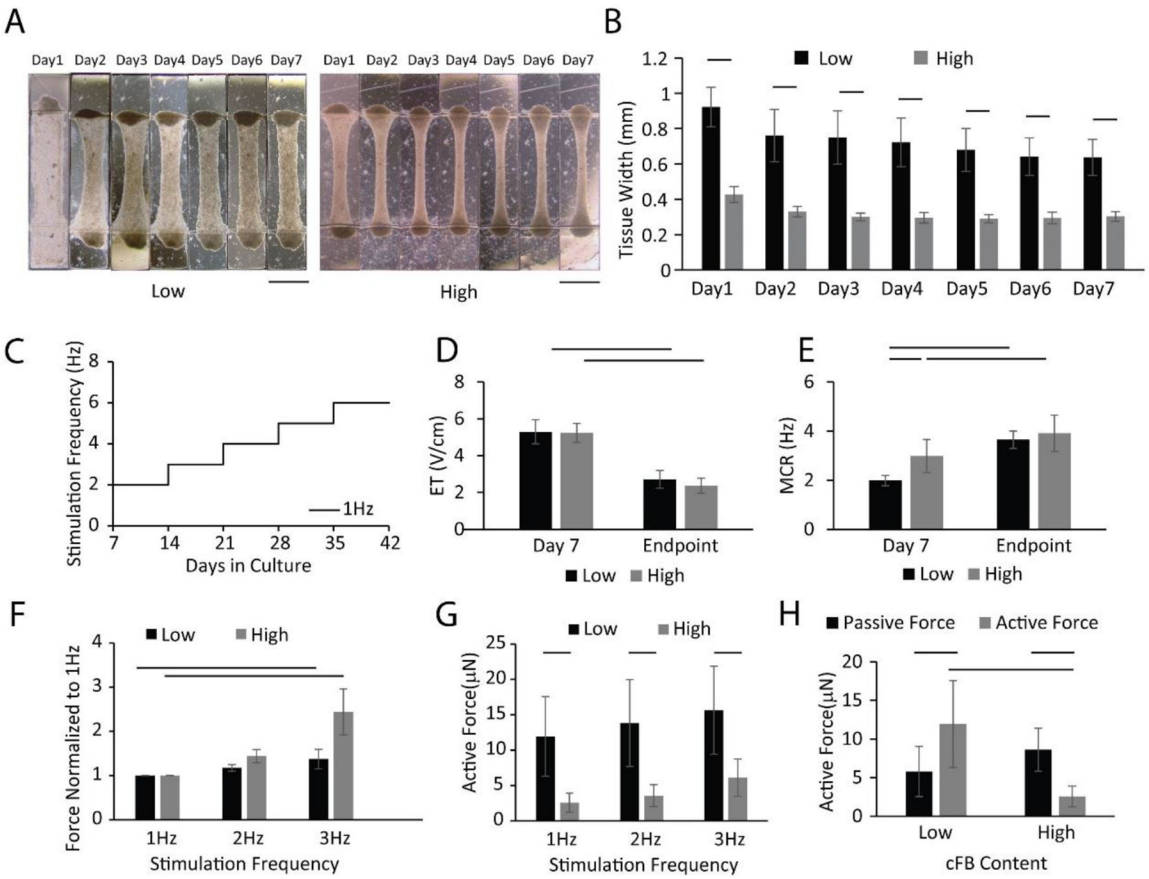

Figure 4: Cardiac fibroblast percentage influences tissue function.

HES3 ESC derived ventricular tissues were seeded in collagen hydrogel with an additional 10% (low cFB group) or 25% (high cFB group) of cardiac fibroblasts. A) Brightfield images of the tissue structure. B) Tissue compaction (n⩾10) in the first week. Electrical stimulation was initiated on day 7 after seeding and the protocol shown in C) was used. D) Excitation threshold (ET) and E) Maximum capture rate (MCR) (n = 7–14) were compared before and after electrical conditioning. Positive Force-frequency relationship (FFR) (n=7 for high cFB group and n=13 for the low cFB group) was shown with F) active forces normalized to 1 Hz. Differences between two groups were demonstrated by G) active forces stimulated at 1–3 Hz at the endpoint of cultivation. H) Active force and passive tension were also compared for both groups. Data are presented as mean ± stdev, Student's t-test or Mann-Whitney test or ANOVA on ranks with Dunn's multiple comparisons test.

Author Manuscript Author Manuscript Author Manuscript Author Manuscript

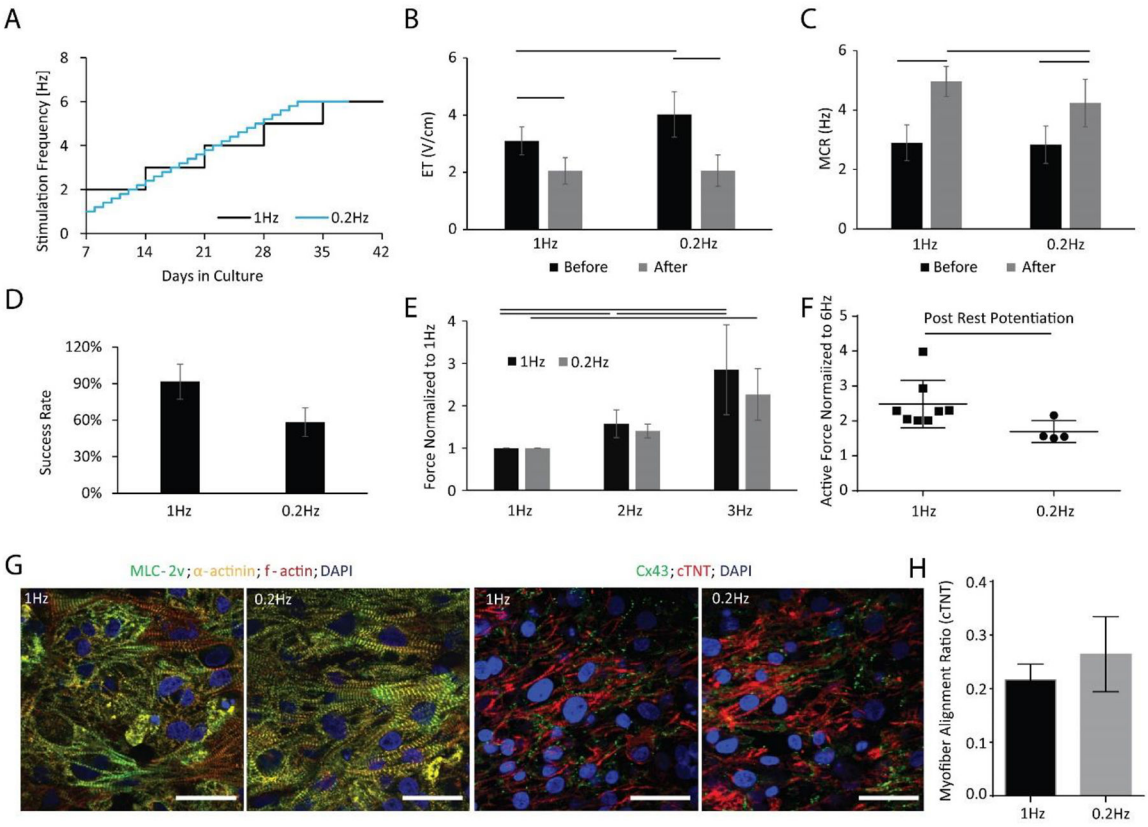

Figure 5: Biowire II platform can generate high fidelity tissues using different stimulation schemes.

A) BJ1D iPSC derived ventricular tissues were conditioned with 1 Hz weekly stimulation regimen or 0.2 Hz daily stimulation regimen. Quantitative comparison of B) Excitation Threshold (ET), (n⩾8) and C) Maximum Capture Rate (MCR), (n≥8). D) Percent of tissues successfully reaching a positive FFR at the end of cultivation (n≥6 for two batches of tissues). E) Force-Frequency Relationship (FFR), (n≥8), F) Post-Rest Potentiation (PRP), (n⩾4). Data presented as mean ± stdev, Student's t-test or two-way ANOVA with Tukey's multiple comparisons test. G) Confocal images of tissues stained for α-actinin, myosin light chain-2v (MLC2v) and F-actin and counterstained with the nuclear stain DAPI (left panels); and stained for connexin-43 (Cx43) and cardiac troponin-T, counterstained with DAPI (right panels). Scale bar=30 μm. H) Quantification of myofiber alignment using cTNT staining. (n=3) Data presented as mean ± stdev, Student's t-test or Mann-Whitney test or One-way ANOVA with Tukey's multiple comparisons test.

Author Manuscript Author Manuscript Author Manuscript Author Manuscript

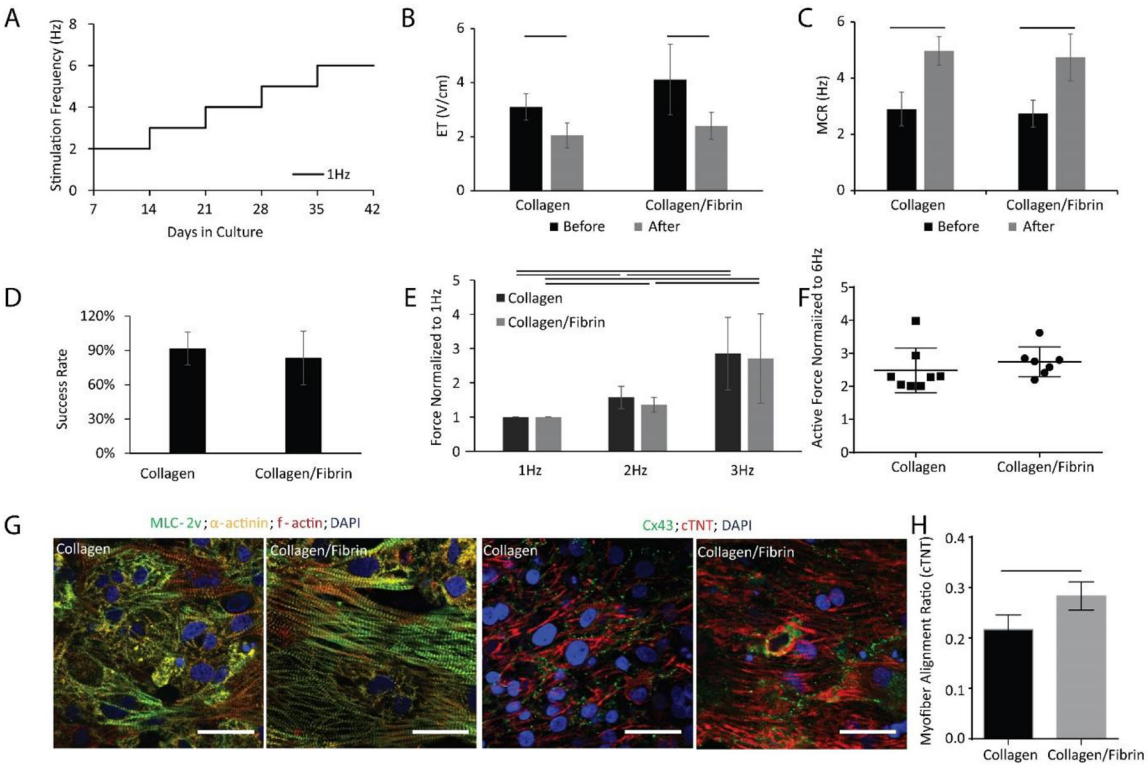

Figure 6: Biowire II platform can generate high fidelity tissues using different hydrogels.

BJ1D iPSC derived ventricular tissues were electrically stimulated as shown in panel A). Quantitative comparison of B) Excitation Threshold (ET), (n⩾8), C) Maximum Capture Rate (MCR), (n⩾8), D) Percent of tissues successfully reaching a positive Force-Frequency Relationship (FFR) by the end of cultivation (two batches of tissues), E) FFR, F) Post-Rest Potentiation (PRP) for tissues generated using Collagen vs. Collagen/Fibrin hydrogel (n⩾7). Data presented as mean ± stdev, Student's t-test or two-way ANOVA with Tukey's multiple comparisons test. G) Confocal images of tissues generated from Collagen vs. Collagen/Fibrin hydrogel stained with for α-actinin, myosin light chain-2v (MLC2v) and F-actin stain, and counterstained with the nuclear stain DAPI (left panels); and stained for connexin-43 (Cx43) and cardiac troponin T (cTNT), counterstained with DAPI (right panels). Scale bar=30 μm. H) Quantification of myofiber alignment using cTNT staining. (n=3). Data presented as mean ± stdev, Student's t-test or Mann-Whitney test or ANOVA on ranks with Dunn's multiple comparisons test.